Water into Wine: Converting Scanner RGB to Tristimulus XYZ

Brian A. Wandell
Department of Psychology
Stanford University
Stanford, CA 94305

J. E. Farrell
Hewlett-Packard Laboratories
1501 Page Mill Road
Palo Alto, CA 94304

April 13, 1994

ABSTRACT

A simple method of converting scanner (RGB) responses to estimates of object tristimulus (XYZ) coordinates is to apply a linear transformation to the RGB values. The transformation parameters are selected subject to minimization of some relevant error measure. While the linear method is easy, it can be quite imprecise. Linear methods are only guaranteed to work when the scanner sensor responsivities are within a linear transformation of the human color-matching functions.

In studying the linear transformation methods, we have observed that the error distribution between the true and estimated XYZ values is often quite regular: plotted in tristimulus coordinates, the error cloud is a highly eccentric ellipse, often nearly a line. We will show that this observation is expected when the collection of surface reflectance functions is well-described by a low-dimensional linear model, as is often the case in practice. We will discuss the implications of our observation for scanner design and for color correction algorithms that encourage operator intervention.

1 INTRODUCTION

There is a gap between the precise color calibration demanded by current software architecture and the data provided by most desktop scanners. For example, Adobe (Postscript Level II) and Apple (ColorSync) have introduced software designed to work

best with digital images represented using calibrated color standards. Yet, most desktop scanners do not have sensors that conform with color measurement standards. Rather, the sensor spectral responsivities and scanner illuminants are designed based on a variety of technical and marketing constraints.

To bridge this gap, system developers have sought computational methods for converting the uncalibrated RGB values into calibrated XYZ methods. Systems developers can choose from a toolbox of calibration methods depending on the job requirements.

The most precise calibration method is to measure everything. If the set of source materials is known in advance, then one can measure the corresponding RGB and XYZ values of the source material. If the process is automated, and if look-up table size is not a significant issue, then calibration can be essentially exhaustive. Exhaustive calibration of a single set of source materials cannot be surpassed for precision; after all you have measured everything that there is to know. But, the total cost may be prohibitive. If exhaustive calibration is impossible, or simply too, well, exhausting, one can still measure finely and use an interpolation rule that is appropriate for three-dimensional interpolation [1].

At the other extreme, the second simplest calibration method, is to use a linear transformation to map sample RGB values into estimated sample XYZ values [2, 3]. [1] Linear transformations are only guaranteed to work well in two cases. The first case is when the scanner sensors are within a linear transformation of the source material tristimulus representation [4]. In this case, we say the scanner is *colorimetric*. As we noted above, however, manufacturers are not building such scanners for the desktop.

There is a second case in which a linear transformation produces accurate results: if the source material surface reflectance functions fall within a three dimensional linear model. If the surfaces are restricted in this way, then one can obtain perfectly calibrated results from any three independent sensors [5, 6].

In practice, surface reflectance functions and scanners do not meet either of these two conditions precisely. Consequently, linear transformations applied to scanners can produce significant amounts of error. As part of a general study of scanner calibration [2] we noticed that the difference between estimated and true XYZ values, when we using linear transform methods, are surprisingly regular. We were motivated to write this paper because we think this regularity may provide system developers with another tool for their color calibration toolbox.

We illustrate the regularity of the error distribution in Figure 1. We scanned the RGB values of targets with known tristimulus coordinates XYZ (under illuminant D_{65}). We then found the linear transformation that minimizes the root mean squared error between the known and estimated XYZ values. We plot the difference between the

[1] The simplest method is to do nothing.

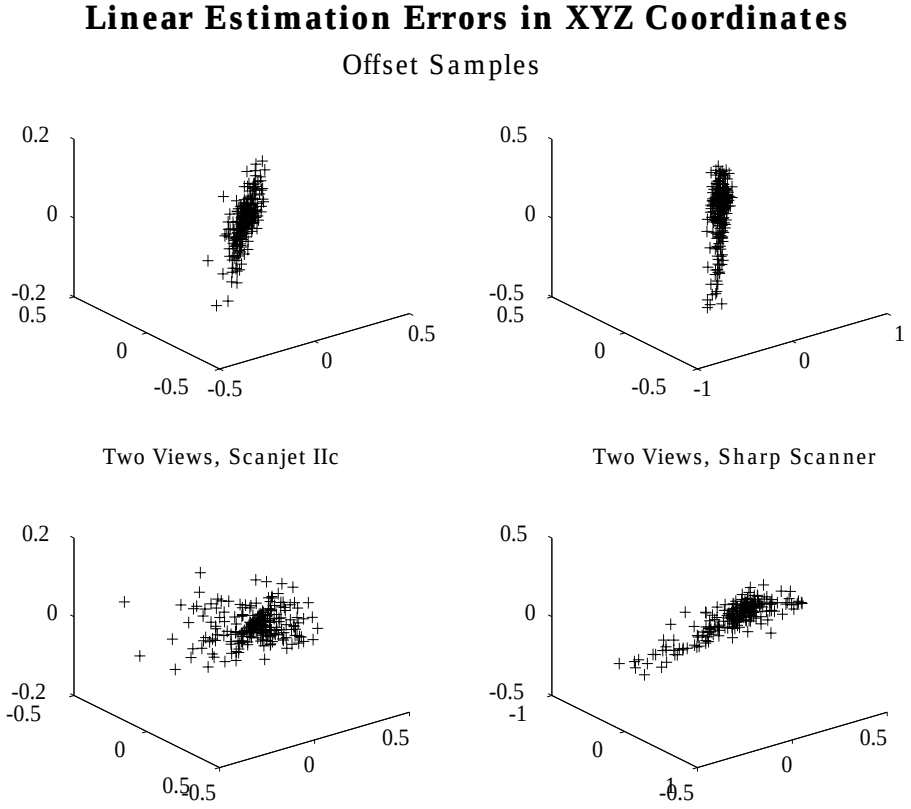

Figure 1: We have derived the best estimate of sample XYZ from scanner RGB for a collection of 214 offset print samples using two different scanners. This figure plots the three-dimensional error cloud of the XYZ estimates for a Hewlett-Packard ScanJet IIc (on the left) and a Sharp JX450 scanner (on the right). The error clouds are shown from two points of view to help the reader see the overall shape. In both cases, and in all cases we have tested, the error cloud is principally elongated in one direction.

known and estimated tristimulus value as a point in three dimensional space in panel (a) of Figure 1. The error cloud is an eccentric ellipsoid; the typical error is much greater in one direction than the other two. We have observed this pattern repeatedly for many sample sets and several different scanners. The directions of the main axes of the ellipsoid vary with the samples and scanner, but the large eccentricity of the ellipsoid reappears again and again.

As we will discuss and illustrate later, the same pattern of results also occurs if one selects the linear transformation from RGB to XYZ subject to minimization of the CIELAB ΔE_{ab} measure and then plots the errors in CIELAB coordinates.

In this report we answer two questions about our observation. First, we wondered whether the property of the error distribution can be derived from considering scanner and sample properties. In the **Proof** section we show the result is expected when surface reflectance functions in the sample collection fall close to a low-dimensional linear subspace. Second, we wondered whether there is some way to take advantage of this structure. In the **Applications** section we consider some implications for software and scanner design.

2 Proof of Main Result

2.1 Notation

We wish to calculate the linear transformation, $L_{3\times 3}$, that maps the scanner RGB values into the surface XYZ value under a standard illuminant, $E(\lambda)$. Place the RGB values in a matrix $R_{3\times N}$ and the XYZ values in a corresponding matrix $X_{3\times N}$. We calculate L by minimizing the quantity

$$\|LR - X\| \quad . \tag{1}$$

The matrix L that minimizes Equation 1 is obtained from the pseudo-inverse of R, $R^+ = R^t(RR^t)^{-1}$ and setting $L = XR^+$. By substituting for X and R we can express the general dependence of L on the surface samples as

$$L = XR^t(RR^t)^{-1} \tag{2}$$

2.2 The transformation's dependence on the samples

The solution, L, depends on the sample reflectance functions we use to perform the calibration. We make this dependence explicit as follows.

Assume the surfaces are perfectly diffuse, and create a matrix $S_{M\times N}$ whose columns contain the N surface reflectance functions sampled at M wavelengths. We calculate the matrix, X, of XYZ values by multiplying S times the matrix $H_{3\times M}$ whose rows are $\bar{x}(\lambda)E(\lambda)$, $\bar{y}(\lambda)E(\lambda)$ and $\bar{z}(\lambda)E(\lambda)$, i.e., $X = HS$. Finally, we assume the scanner is linear with a transfer matrix is $T_{3\times M}$. The matrix, R, of RGB values is $R = TS$.

By substituting for X and R into Equation 2 we can express the general dependence of L on the surface samples as

$$\begin{aligned} L &= HS(TS)^t(TS(TS)^t)^{-1} && (3)\\ &= H(SS^t)T(TSS^tT^t)^{-1} \quad . && (4) \end{aligned}$$

In general, the best linear transformation depends on the set of samples in our measurement set through the covariance matrix, SS^t. When the surface reflectance functions form an orthonormal basis set, so that $SS^t = I_{M\times M}$, Equation 3 simplifies to

$$L = HT^t(TT^t)^{-1} \quad . \tag{5}$$

2.3 Error vectors when the samples are in a linear subspace

Now we show how L, and thus the error vectors $LR - X$, depend on the samples when the surface reflectances fall within a four dimensional linear model.

We say that the surface reflectance functions fall within a four-dimensional linear model when there exist four basis functions, the columns of $\hat{S}_{M\times 4}$, and a set of four-dimensional model-weights, the columns of $W_{4\times N}$ with $WW^t = I_{4\times 4}$, such that $S = \hat{S}W$. We substitute the linear model representation of S in Equation 3 to obtain

$$L = H\hat{S}W(T\hat{S}W)^t(T\hat{S}W(T\hat{S}W)^t)^{-1} \quad . \tag{6}$$

We reduce the number of symbols by defining $A_{3\times N} = T\hat{S}$ and $B_{3\times N} = H\hat{S}$ and obtain

$$L = BA^t(AA^t)^{-1} \quad . \tag{7}$$

Finally, express the error vectors in terms of the matrices A and B using

$$\begin{aligned} X - LR &= X - BA^t(AA^t)^{-1}R && (8)\\ &= BW - BA^t(AA^t)^{-1}AW && (9)\\ &= B(I_{N\times N} - A^t(AA^t)^{-1}A)W \quad . && (10) \end{aligned}$$

(Remember, by definition $R = AW$ and $X = BW$).

We see that the error vectors are a linear transformation of the four-dimensional model-weights describing the surfaces, W. The matrix $P_A = A^t(AA^t)^{-1}A$ projects the four-dimensional vectors of model-weights into a three-dimensional subspace spanned by the rows of A. The matrix P_A has rank 3 when the rows of A are independent (i.e. A has rank 3). The matrix $I_{N\times N} - P_A$ maps the four-dimensional vectors of surface weights into the orthogonal complement to the rows of A; so the rank of $I - P_A$ must be 1. The matrix B has rank of 3, so it follows that that the matrix of errors, $X - LR$, has rank one.

This proves our main result: when the surface reflectances fall within a four-dimensional linear model, the errors of the best linear estimates of the sample XYZ values must fall within a one-dimensional subspace. [2]

2.4 Discussion of the Proof

Our proof explains why there is a strong tendency for the errors measured in XYZ coordinates to follow distended ellipses. As Wandell and Brainard [7] observed for print samples and others have observed for many other surface collections [8, 9, 10], surface reflectances of many objects are well-described by low-dimensional linear models. Figure 2 shows the first five terms in the least-squares linear model approximation of the surface reflectances in the offset print samples we used. The figure illustrates that for the 214 offset samples, there is very little variance left to explain by the fifth term; since a four-dimensional linear model does well at explaining the reflectance functions, the theorem suggests that the errors should fall near a one-dimensional subspace [3].

The results we obtained apply to errors measured in XYZ coordinates. In many applications, we may be interested in the the errors measured in a perceptually uniform space. Transformations into CIELAB or CIELUV space are non-linear, and we have not obtained analytic results for this case. However, since the XYZ error vectors are modest in size, and the transformations are locally smooth, it is not surprising that when we plot the error vectors plotted in CIELAB space the error vectors continue to scatter along a distended ellipsoid. The relative significance of different errors is changed, but the overall pattern remains following the transformation into CIELAB.

We illustrate the scatter for the offset samples and a Macbeth Color-Checker in the two panels of Figure 3. We selected linear transformations from the scanner RGB values to the sample XYZ values in order to minimize the mean ΔE_{ab} error between the observed and predicted XYZ values. For the offset samples, the ΔE_{ab} values for

[2] It can also be shown that when the surface reflectance functions fall in a five dimensional subspace the errors must fall in a two-dimensional subspace.

[3] Except if the scanner or human visual system greatly amplify the effects of the higher order terms compared to the lower order. See the discussion in [11]

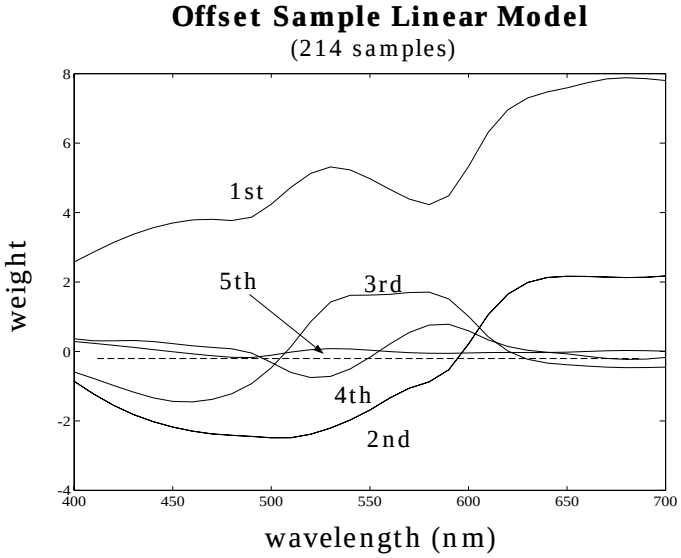

Figure 2: These curves are the first five terms in a linear model designed to minimize the root mean squared error in predicting the reflectance functions of the offset samples. The curves were calculated as the first five left singular vectors of the matrix S, each multiplied by the corresponding singular value. The height of each curve suggests its relative importance in describing the data set.

the mean value was 3.326 (max = 10.813). For the Macbeth samples the mean was 3.649 (max = 13.147). The Figure illustrates that the error clouds remain rather elliptical even in this nonlinear representation of the data.

3 Applications

3.1 Software design

Much of the user satisfaction from using a color scanner comes from the ability to manipulate the color appearance of the scanner data. Beyond this, since nearly all scanners on the market fail to reproduce some original colors accurately, on some occasions users need to manipulate the data to make it match the original. Hence, scanner calibration software should provide the user with the mean to correct, as well as to enhance, the colors in a scanned image.

One of the more confusing aspects of color software adjustment arises because the user must search through a three-dimensional color representation to select an appropriate color. Searches through the three-dimensional color space, with all the buttons, knobs, and jargon, can be confusing.

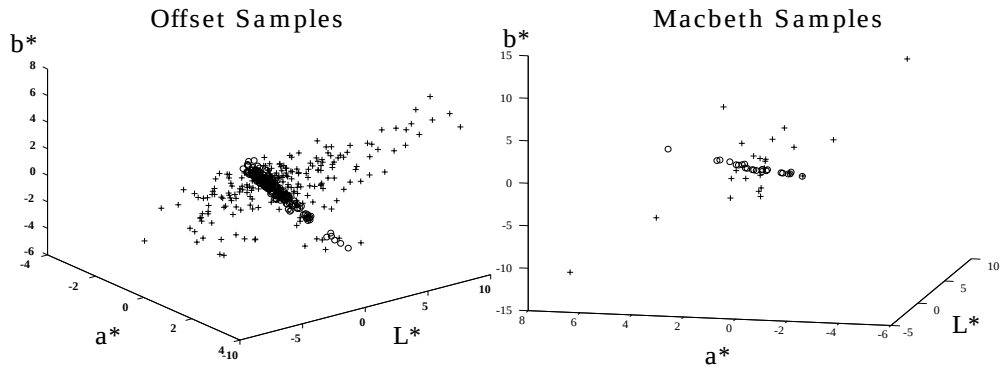

Figure 3: The crosses plot the error vector in CIELAB when the sample XYZ value is predicted by a linear transformation of the scanner RGB. The linear transformation was selected by minimizing the root mean squared error in CIELAB space (i.e. ΔE_{ab}). The circles show the best correction we can obtain when we eliminate the error in one dimension, as described in the text; the circles fall on a plane perpendicular to the principal axis of the ellipse in CIELAB space, although this is not easy to see in a single projection. The data were measured on the HP ScanJet IIC, using the offset samples (left) and the Macbeth color-checker (right).

Scanner	*Sample*	*Linear*	*Corrected*
HP	Macbeth	3.649 (13.147)	1.719 (6.183)
Sharp	Macbeth	4.914 (13.592)	2.359 (6.190)
HP	Offset	3.326 (10.813)	1.826 (6.457)
Sharp	Offset	6.017 (19.624)	2.367 (8.800)

Table 1: The first column describes the scanner and the second column the samples. Mean and maximum linear errors, based on the linear transformation that minimizes mean ΔE_{ab}, are shown in column 3. The mean (max) estimation errors after removing the principal error dimension are shown in column 4.

Our results may be of some practical value since they suggest a way to simplify color correction. Since most of the error is oriented along a particular direction in both XYZ and CIELAB space, we can design modules to help the user eliminate the error through a guided search along the one dimension with the largest error. The user can select a region and adjust the color using a slider that changes the color along a line in CIELAB coordinates. The line in color coordinates is selected based on calibration of the scanner and source materials; we select the line where most of the calibration error occurs. Rather than searching through a two or three-dimensional color space as is commonplace, (see, for example, Cachet, manufactured and sold by EFI), the user can remove most of the error using a one-dimensional slider.

How effective will a constrained one-dimensional color correction be? We have examined this process visually on a color monitor and we will present examples in our talk. we adjusted the CIELAB values predicted by the Sharp JX450 scanner in the direction corresponding to the major axis of the elliptical error, minimizing the difference between the predicted CIELAB values and the measured CIELAB values, for 214 samples of color offset lithography. Before the one-dimensional correction, the mean ΔE_{ab} error was 6.0174 (max = 19.6241). After the one-dimensional color correction, the mean ΔE_{ab} error was 2.3665 (max = 8.8). The error can be made even smaller, of course, if we perform a second constrained adjustment.

Table 3.1 lists the improvements for the four combinations of Macbeth samples and the HP and Sharp scanners.

3.2 Scanner design

A final implication of our observations is that the addition of a fourth sensor to conventional scanners can reduce the observed error considerably. The addition of a fourth scanner will permit algorithms to remove the error in the largest dimension. The results in Table 3.1 can also be seen as describing how much the color error can be

reduced by the addition of a fourth sensor. Our observation supports arguments about scanner color reproduction by Vrhel and Trussell [12]

4 Conclusions

Linear transformations that map scanner RGB values into estimates of sample XYZ are inexpensive but inaccurate. But, the XYZ errors typically fall near a line that is characteristic of the scanner and the sample set. This property is expected when the sample set surface reflectance functions fall near a four-dimensional subspace. Schemes in which the user adjusts the estimated color manually in three dimensions to match the true color can be complex and frustrating. It is possible to provide users a simple means of improving the principal color error by a guided correction mechanism; the observer adjusts a slider that corrects the estimated color along the axis defined by the principal error direction.

5 Acknowledgments

We thank D. Marimont for comments and providing us with a simplification of our original proof. We thank E.J. Chichilnisky for comments. Supported by NEI RO1 EY03164 and NASA 2-307.

References

[1] P. Hung. Colorimetric calibration for scanners and media. In *SPIE Conference Proceedings San Jose*, pages 164–174. SPIE, February 1991. Contact Rochester Institute of Technology color lab.

[2] J. Farrell, J. Meyer, R. Motta, B. Wandell, and E. Chichilnisky. Sources of scanner calibration errors. In *IS&T's Eight International Congress on on Advances in Non-impact Printing Technologies*, 1992.

[3] P. Roetling, J. Stinehous, and M. Maltz. Color characterization of a scanner. *Procedings of the IS and T (Portland)*, 1991.

[4] G. Wyszecki and W. S. Stiles. *Color Science*. John Wiley and Sons, New York, second edition, 1982.

[5] B. K. P. Horn. Exact reproduction of colored images. *Computer Vision, Graphics and Image Processing*, 26:135–167, 1984.

[6] B. A. Wandell. Color rendering of camera data. *Col. Res. Appl., Supplement*, 11:S30–S33, 1986.

[7] B. A. Wandell and D. H. Brainard. Towards cross-media color reproduction. In *Proceedings OSA applied vision topical meeting*. Optical Society, San Francisco, CA, 1980b.

[8] J. Cohen. Dependency of the spectral reflectance curves of the munsell color chips. *Psychon. Sci*, 1:369–370, 1964.

[9] L. T. Maloney. Evaluation of linear models of surface spectral reflectance with small numbers of parameters. *J. Opt. Soc. Am. A*, 3:1673–1683, 1986.

[10] J. P. S. Parkkinen, J. Hallikainen, and T. Jaaskelainen. Characteristic spectra of munsell colors. *J. Opt. Soc. Am.*, 6:318–322, 1989.

[11] D. Marimont and B. Wandell. Linear models of surface and illuminant spectra. *J. Opt. Soc. Am. A*, 11:1905–1913, 1992.

[12] M. J. Vrhel and H. J. Trussell. Filter considerations in color correction. In *SPIE Symposium on Electronic Imaging*, San Jose, CA, February 1992.